Universal Visual Decomposer: Long-Horizon Manipulation Made Easy

Zichen Zhang[*1], Yunshuang Li[*2], Osbert Bastani[2], Abhishek Gupta[3],

Dinesh Jayaraman[2], Yecheng Jason Ma[†2], Luca Weihs[†1]

zcczhang.github.io/UVD

Abstract— Real-world robotic tasks stretch over extended horizons and encompass multiple stages. Learning long-horizon manipulation tasks, however, is a long-standing challenge, and demands decomposing the overarching task into several manageable subtasks to facilitate policy learning and generalization to unseen tasks. Prior task decomposition methods require task-specific knowledge, are computationally intensive, and cannot readily be applied to new tasks. To address these shortcomings, we propose Universal Visual Decomposer (UVD), an off-the-shelf task decomposition method for visual long-horizon manipulation using pre-trained visual representations designed for robotic control. At a high level, UVD discovers subgoals by detecting phase shifts in the embedding space of the pre-trained representation. Operating purely on visual demonstrations without auxiliary information, UVD can effectively extract visual subgoals embedded in the videos, while incurring zero additional training cost on top of standard visuomotor policy training. Goal-conditioned policies learned with UVD-discovered subgoals exhibit significantly improved compositional generalization at test time to unseen tasks. Furthermore, UVD-discovered subgoals can be used to construct goal-based reward shaping that jump-starts temporally extended exploration for reinforcement learning. We extensively evaluate UVD on both simulation and real-world tasks, and in all cases, UVD substantially outperforms baselines across imitation and reinforcement learning settings on in-domain and out-of-domain task sequences alike, validating the clear advantage of automated visual task decomposition within the simple, compact UVD framework.

I. INTRODUCTION

Real-world household tasks, such as cooking and tidying, often stretch over extended horizons and encompass multiple stages. In order for robots to be deployed in realistic environments, they must possess the capability to learn and perform long-horizon manipulation tasks from visual observations. Learning vision-based complex skills over long timescales, however, is challenging due to the problem of compounding errors, the vastness of the action and observation spaces, and the difficulty in providing meaningful learning signals for each step of the task.

Given these challenges, it is necessary to *decompose* a long-horizon task into several smaller subtasks to make learning manageable. Beyond improving the efficiency of learning, task decomposition facilitates learning reusable skills, promotes data-sharing across different trajectories, and further enables compositional generalization to unseen sequences of the learned subtasks. Despite its usefulness, task

*Equal Contribution. †Equal Advising

[1]Allen Institute for AI, [2]University of Pennsylvania, [3]University of Washington
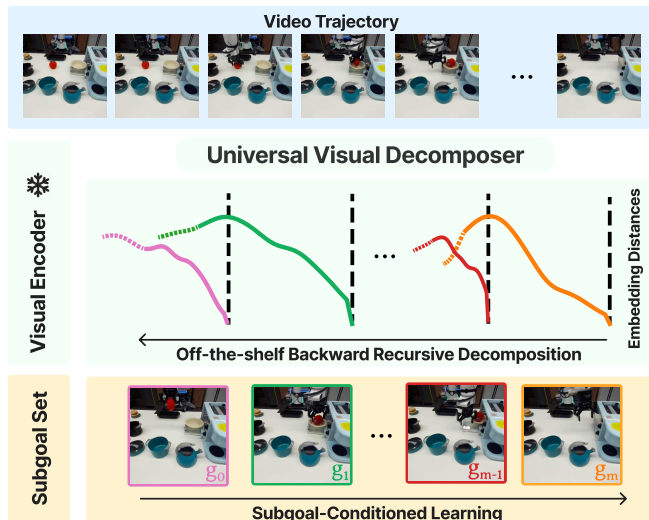
Fig. 1: **Universal Visual Decomposer** uses off-the-shelf pre-trained visual representations to find subgoals from video demonstrations by recursively computing embedding distances from the target goal and setting the first plateau as the new target goal.

decomposition is difficult to perform in practice, and most existing approaches require strong assumptions about tasks, datasets, or robotic platforms [3,12,13,20,21,34,37,43,49–51,61]. These methods cannot be used in common settings where the agent only has access to video demonstrations of desired behavior on their robotic hardware and little else, motivating the need for an off-the-shelf approach that can readily decompose *any* visual demonstration out-of-the-box.

In order to decompose any long-horizon task using vision, general knowledge about visual task progression that can discern embedded subtasks in long, unsegmented task videos must be acquired. In this work, we propose Universal Visual Decomposer (UVD), an off-the-shelf unsupervised subgoal decomposition method that re-purposes state-of-the-art pre-trained visual representations [24,31–33,38,42,60] for automated task segmentation. To motivate our approach, we observe that several pre-trained visual representations, such as VIP [32] and R3M [38], are trained to capture temporal task progress on diverse, short videos of humans accomplishing goal-directed behavior [7,15]. These representations have acquired well-behaved embedding distances that can progress near *monotonically* along video frames that depict short-horizon, atomic skills. Our key insight is that when applied to long videos consisting of several subtasks, their training

on short atomic tasks makes these representations no longer informative about subtask membership. That is, they are not trained to capture whether an earlier frame, which may very well belong to a different subtask, is making progress towards a subtask that appears later in the video, even if the subtasks are related to one another. As a consequence, when the robot task is extended, the embedding distances will *deviate* from monotonicity and exhibit plateaus around frames that correspond to phase shifts in the overall task; this provides an unsupervised signal for detecting when subtasks have taken place in the original long, unsegmented task video. UVD instantiates this insight and proposes an out-of-the-box subgoal discovery procedure that can iteratively extract subgoals using the embedding distance information from the end to the beginning; notably, UVD does not require any domain-specific knowledge or incur additional training cost on top of standard visuomotor policy training. Given its off-the-shelf nature, UVD can be readily applied to a variety of unseen robot domains. See Fig. 1 for a conceptual overview of our approach.

We apply UVD to long-horizon, multi-stage visual manipulation tasks in both simulation and real-world environments. Across these tasks, UVD consistently outputs semantically meaningful subgoals which are used for policy training and evaluation. We consider both in-domain (IND) and out-of-domain (OOD) task evaluations. In IND evaluation, the agent is evaluated on long-horizon tasks for which it has been explicitly trained whereas in OOD evaluation, the agent is evaluated to generalize to new tasks unseen during training. Using UVD-discovered subgoals, we demonstrate substantial policy improvements across these evaluation settings. Firstly, when training agents with reinforcement learning (RL), we show that UVD-subgoals can be used to perform *reward shaping* for each of the intermediate subtasks. Using this approach, we demonstrate that the resulting rewards can successfully guide a vision-based reinforcement learning agent to learn long-horizon tasks in the FrankaKitchen [16] environment. Secondly, when training agents with imitation learning (IL), by virtue of discovering semantically meaning subgoals, our policies can *compositionally generalize* to OOD task sequences unseen during training; this capability greatly reduces the burden of manual data collection for every desired task. Finally, in IND evaluation, we also demonstrate performance improvement on several real-world multi-stage tasks that stretch over several hundred timesteps and exhibit sequential dependency among the subtasks.

In summary, our contributions include:

1) Universal Visual Decomposer (UVD), an off-the-shelf visual decomposition method for long-horizon manipulation using pre-trained visual representations.
2) A reward shaping method for long-horizon visual reinforcement learning using UVD-discovered subgoals.
3) Extensive experiments demonstrating UVD's effectiveness in improving policy performance on IND and OOD evaluations across several simulation and real-robot tasks.

II. RELATED WORK

Learning long-horizon skills has been a long standing challenge in robotic manipulation [16,19,26,34]. Hierarchical reinforcement learning [1,2,4,6,11,16,35,36,39,50,54,64] enables temporally extended exploration by discovering subskills and planning over them. However, these algorithms learn subskills and overall policies from scratch, which is computationally expensive and less suitable for real-world robotics use cases.

When provided with task demonstrations, there are many prior efforts on using subgoal decomposition as a means to break up the long task in order to provide intermediate learning signals and to mitigate compounding action errors. These prior decomposition strategies, however, require task-specific knowledge and cannot be easily applied to new tasks. For example, several approaches use the robot's proprioceptive data within the task demonstrations [3,21,49,51] or explicit knowledge about subtask structure [20,61] to guide decomposition; this limits the types of tasks that can be solved and precludes learning from observed videos. Other works learn latent generative models over subgoals [12,13,22,34,37,43], but demand compute-intensive training on large datasets that cover diverse behavior.

To the best of our knowledge, Universal Visual Decomposer is the first "off-the-shelf" visual task decomposition method that does not require any task-specific knowledge or training. In addition, it demonstrates a novel use case of pre-trained visual representations. While some prior works have considered using pre-trained visual representations to generate rewards [32,47], we are the first to demonstrate that they can also be re-purposed to perform hierarchical decomposition; furthermore, this capability can be combined with the reward specification capability to solve long-horizon tasks using visual reinforcement learning.

III. PROBLEM SETTING

Unsupervised Subgoal Discovery (USD). Our goal is to derive a general-purpose subgoal decomposition method that can operate purely from visual inputs on a *per-trajectory* basis. That is, given a full-task demonstration $\tau = (o_0, ..., o_T)$,

$$\text{USD}((o_0, ..., o_T)) \rightarrow \tau_{goal} := (g_0, ..., g_m), \quad (1)$$

where $(g_0, ..., g_m)$ are the subset of τ that are selected as subgoals; m may vary across trajectories.

Policy Learning. We provide demonstrations $\mathcal{D} := \{\tau\}_{i=1}^n$ for the learning tasks; in the reinforcement learning setting, we assume that there is one task and have $n = 1$ to specify the overall task to be achieved. The evaluation tasks can be both in-domain (IND), the ground-truth sequences of tasks captured in $\mathcal{D}$, or out-of-domain (OOD), consisting of unseen combinations of the subtasks in $\mathcal{D}$.

We assume access to a pre-trained visual representation $\phi : \mathbb{R}^{H \times W \times 3} \rightarrow \mathbb{R}^K$ that maps RGB images to a K-dimensional embedding space. Given ϕ and $\mathcal{D}$, our goal is to learn a goal-conditioned policy $\pi : \mathbb{R}^K \times \mathbb{R}^K \rightarrow \Delta(A)$ that outputs an action based on the embedded observation and goal, $a \sim \pi(\phi(o), \phi(g))$. In the RL setting, the agent is not provided

with reward information, so the agent must also construct rewards using ϕ and $\mathcal{D}$.

Policy Evaluation. For OoD eval., we provide one demonstration τ specifying the subtask sequence to be performed.

IV. METHOD

We first present Universal Visual Decomposer, the core algorithm that powers our off-the-shelf subgoal discovery approach. Then, we discuss various ways we perform policy training as well as goal selection during policy inference.

A. Universal Visual Decomposer

Given an unlabeled video demonstration $\tau = (o_0, ..., o_T)$, how might we discover useful subgoals? The key intuition of Universal Visual Decomposer is that, conditioned on a goal frame o_t, some n frames $(o_{t-n}, ..., o_{t-1})$ preceding it must visually approach the goal frame; once we discover the first frame (o_{t-n}) in this goal-reaching sequence, the frame that precedes it (o_{t-n-1}) is then another subgoal. From o_{t-n-1}, the same procedure can be carried out *recursively* until we reach o_0. There are two central questions to address: (1) how to discover the first subgoal (last in terms of timestamp), and (2) how to determine the stopping point for the current subgoal and declare a new frame as the new subgoal.

The first question is simple to resolve by observing that in a demonstration, the last frame o_T is naturally a goal. Now, conditioned on a subgoal o_t, we attempt to extract the first frame o_{t-n} in the sub-sequence of frames that depicts visual task progression to o_t. To discover this first frame, we exploit the fact that several state-of-the-art pre-trained visual representations for robot control [31,32,38] are trained to capture temporal progress within short videos depicting a single solved task; these representations can effectively produce embedding distances that exhibit *monotone* trend over a short goal-reaching video sequence $\tau = (o_{t-n}, ..., o_t)$:

$$d_\phi(o_s; o_t) \geq d_\phi(o_{s+1}; o_t), \forall s \in \{t-n, ..., t-1\}, \quad (2)$$

where d_ϕ is a distance function in the ϕ-representation space; in this work, we set $d_\phi(o; o') := \|\phi(o) - \phi(o')\|_2$ because several state-of-the-art pre-trained representations use the L_2 distance as their embedding metric for learning. Given this, we set the previous subgoal to be the temporally closest observation to o_t for which this monotonicity condition fails:

$$o_{t-n-1} := \arg\max_{o_h} d_\phi(o_h; o_t) < d_\phi(o_{h+1}; o_t), h < t . \quad (3)$$

The intuition is that a preceding frame that belongs to the same subtask (i.e., visually apparent that it is progressing towards o_t) should have a higher embedding distance than the succeeding frame if the embedding distance indeed captures temporal progression. As a result, a deviation from the monotonicity indicates that the preceding frame may not exhibit a clear relation to the current subgoal, and instead be a subgoal itself. Now, o_{t-n-1} becomes the new subgoal, and we apply (3) recursively until the full sequence τ is exhausted. For instance, in Figure 1, conditioned on the last frame, g_3 is the first preceding frame that produces an inflection point in the embedding distances and hence selected as

a subgoal; then, conditioned on g_3, g_2 is selected, and so on; see Alg. 1 for high-level algorithm and Psuedocode A.1 for low-level implementation. In practice, (2) may not hold for every step due to noise in the embedding and pixel space, and we find that a simple pre-set minimal time interval between each decomposed subgoal to ensure they aren't too close together and a low pass filter procedure to first smoothen the embedding distances make the subgoal criterion (3) effective; see Appendix. A for more details.

Algorithm 1: Universal Visual Decomposer

Init: frozen visual encoder ϕ, $\tau = \{o_0, \cdots, o_T\}$
Init: set of subgoals $\tau_{goal} = \{\}$, $t = T$
while t *not small enough* **do**
    $\tau_{goal} = \tau_{goal} \cup \{o_t\}$
    Find o_{t-n-1} from Eq. 3
    $t = t - n - 1$
end

In Fig. 2, we visualize UVD's iterative decomposition process, showcasing the embedding distance curves (left) and the resulting decomposed subgoals (right). The featured videos are sourced from FrankaKitchen for the simulation task, `Fold-cloth` for the real-robot task, and a real-world sequence that includes: opening a drawer, picking the charger, plugging it in, activating the power strip, and partially closing the drawer. The black dotted lines indicate the timesteps where UVD identifies a monotonic break, taking into account the minimal interval mentioned earlier. More visualizations can be found in Appendix F.

Computational Efficiency. We highlight that our entire algorithm does not require any additional neural network training or forward computations on top of the one forward pass required to encode all observations for policy learning. We further provide the decomposition and inference runtime for our UVD implementation in Appendix. 4. The results indicate that UVD introduces negligible costs (< 0.1 sec. in total) when compared to standard policy learning methods.

B. UVD-Guided Policy Learning

Now, we discuss several ways UVD-discovered subgoals can be used to supplement policy learning.

Goal Relabeling. As UVD is performed on a trajectory basis, we can relabel all observations in a trajectory with the closest subgoals that appear later in time. In particular, for an action-labeled trajectory $\tau = (o_0, a_0, ..., o_T, a_T)$ and UVD-discovered subgoals $\tau_{goal} = (g_0, ..., g_m)$, we have that `Label`$(o_t) = g_k$ where g_k is the first subgoal occurring after time t. This procedure leads to an augmented, goal-relabeled trajectory $\tau_{aug} = \{(o_0, a_0, g_0), ..., (o_T, a_T, g_m)\}$. Now, as all transitions are goal-conditioned, we can learn policies using any goal-conditioned imitation learning algorithm; for simplicity, we use goal-conditioned behavior cloning (GCBC) [10,14].

Reward Shaping. The above goal relabeling strategy applies to the imitation learning (IL) setting. Collecting the demonstrations needed for IL is, however, expensive. Instead,
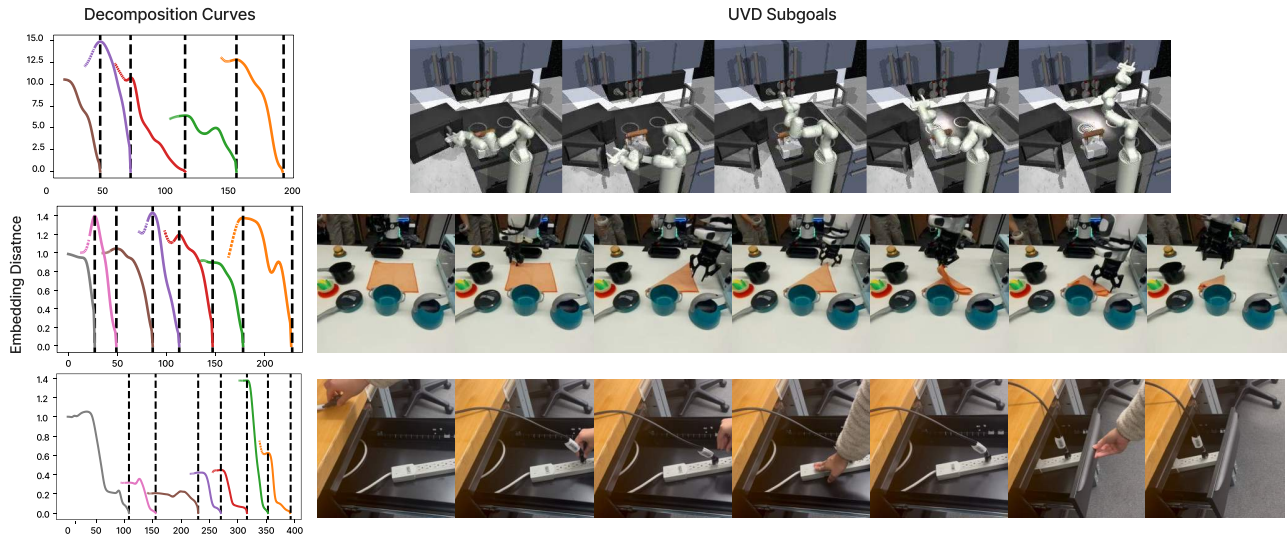
Fig. 2: **Illustrations of UVD's iterative decomposition, showcasing embedding distance curves (left) and decomposed subgoals (right).** The videos come from FrankaKitchen for the simulation task, `Fold-cloth` for the real-robot task, and a real-world video depicting the sequence: opening a drawer, picking the charger, plugging it in, activating the power strip, and partially closing the drawer.

a reinforcement learning paradigm is feasible with much fewer demonstrations and comes with other ancillary benefits such as learned error recovery. This raises the question of how UVD-subgoals might be used with an RL paradigm. In particular, how can UVD help overcome the exploration challenge in long-horizon RL? Given that UVD selects subgoals so that the embedding distances in-between any two consecutive subgoals exhibit monotone trends, we define the *UVD reward* to be the goal-embedding distance *difference* computed using UVD goals:

$$R(o_t, o_{t+1}; \phi, g_i) := d_\phi(o_t; g_i) - d_\phi(o_{t+1}; g_i) . \quad (4)$$

where $g_i \in \tau_{goal}$, and g_i will be switched to g_{i+1} automatically during training when $d_\phi(o_{t+1}; g_i)$ is small enough. More details can be found at Appendix. 2.. This choice of reward encourages making consistent progress towards the goal and has been found in prior work [8,32,57,59] to be particularly effective when deployed with suitable visual representations.

C. UVD Goal Inference

When deploying our trained subgoal-conditioned policies at inference time, we must determine what subgoals to instruct the policy to follow at each observation step. We study two simple strategies that work well in practice; we describe the high-level approaches here, and include more details on Appendix. 2..

Nearest Neighbor. First, when there is only one fixed sequence of subtasks to be learned (*i.e.*, IND), we employ a simple nearest neighbor goal selection strategy. That is, for a new observation, we compute the observation in the training set that has the closest embedding (judged by d_ϕ) and use its associated sub-goal. This can be interpreted as a

non-parameteric high-level policy that outputs observation-conditioned goal for the low level policy, $\pi(\phi(o), \phi(g))$.

Goal Relaying. When performing OOD or multi-task IND evaluation, the agent must complete a user-instructed task. In these settings, the above nearest neighbor approach may no longer apply as the subgoals seen in training may not be valid for the current, potentially unseen, task. Instead, we propose to relay the currently instructed goals based on embedding distance. Specifically, given a sequence of instructed subgoals $g = (g_0, ..., g_m)$, the policy will condition on the first remaining subgoal until the embedding distance between the current observation and the subgoal is below a certain threshold, at which point the policy will be conditioned on the next subgoal in the sequence.

V. EXPERIMENTS

We study the following research questions:

1) Does UVD enable compositional generalization in multi-stage and multi-task imitation learning?
2) Can UVD subgoals enable reward-shaping for long-horizon reinforcement learning?
3) Can UVD be deployed on real-robot tasks?

A. Simulation Experiments

FrankaKitchen Environment. We use the FrankaKitchen Environment [16] for simulation experiments. In the environment, a Franka robot with a 9-DoF torque-controlled action space can interact with seven objects: a microwave, a kettle, two stove burners, a light switch, a hinge cabinet, and a sliding cabinet. We refined the dataset from [16] to include only successful trajectories, yielding a total of 513 episodes gathered from humans using VR headsets. For each episode, four out of the seven objects are manipulated in an arbitrary sequence, leading to 24 unique completion orders; see Fig. 3.

Representation	Method	IND success	IND completion	OOD success	OOD completion
VIP (ResNet50) [32]	GCBC	0.736 (0.011)	0.898 (0.006)	0.035 (0.014)	0.236 (0.057)
	GCBC + Ours	0.737 (0.012)	0.903 (0.009)	**0.188 (0.024)**	**0.566 (0.020)**
R3M (ResNet50) [38]	GCBC	0.742 (0.026)	0.856 (0.006)	0.014 (0.007)	0.223 (0.029)
	GCBC + Ours	0.738 (0.024)	**0.879 (0.000)**	**0.084 (0.045)**	**0.427 (0.002)**
LIV (ResNet50) [31]	GCBC	0.608 (0.068)	0.816 (0.046)	0.008 (0.008)	0.116 (0.082)
	GCBC + Ours	**0.649 (0.013)**	**0.868 (0.007)**	**0.066 (0.025)**	**0.496 (0.033)**
CLIP (ResNet50) [25]	GCBC	0.391 (0.017)	0.692 (0.008)	0.005 (0.001)	0.119 (0.017)
	GCBC + Ours	0.394 (0.036)	0.701 (0.012)	**0.073 (0.003)**	**0.403 (0.01)**
DINO-v2 (ViT-large) [41]	GCBC	0.329 (0.025)	0.654 (0.019)	0.012 (0.01)	0.261 (0.213)
	GCBC + Ours	0.322 (0.053)	0.669 (0.037)	**0.055 (0.025)**	**0.446 (0.034)**
VIP (ResNet50) [32]	GCBC-GPT	0.702 (0.029)	0.841 (0.02)	0.039 (0.027)	0.302 (0.028)
	GCBC-GPT + Ours	0.708 (0.056)	**0.897 (0.024)**	**0.213 (0.054)**	**0.600 (0.038)**

TABLE I: **IND and OOD IL Results on FrankaKitchen.** We report the mean and standard deviation of success rate (full-stage completion) and the percentage of the completion (out of 4 stages), evaluated over diverse existing pretrained visual representations trained by GCBC with three seeds. Highlighted scores represent improvements in OOD evaluations and IND results with gains exceeding 0.01.
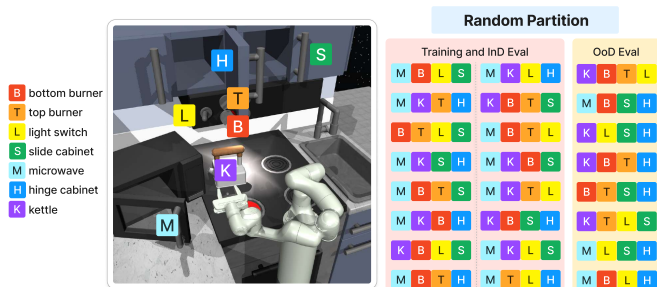

Fig. 3: **Frank Kitchen environment and an example of random training-evaluation partition.** In each demonstration episode, 4 out of 7 objects are manipulated in an arbitrary order. We show an example of 16 completion orders for training and IND evaluation chosen randomly, while the rest of 8 are for OOD generalizations.

Visual and Policy Backbones. As UVD is designed to utilize pre-trained visual representations that capture visual task progress, we adopt R3M [38], VIP [32], and LIV [31], three Resnet50-based representations trained with temporal objectives on video data; in particular, VIP and LIV are trained to explicitly encode smooth temporal task progress in their embedding distances. We also consider general vision models trained on static image datasets such as CLIP (ResNet50) [44] and DINO-v2 (ViT-large) [41] to assess the importance of training on temporal data. As our goal is to study the merit of the pretrained representations, as in prior works [32,38], we keep the policy architecture simple and employ a multi-layer perception (MLP) as the policy architecture; More details in Appendix. B.

Baselines. We compare with goal-conditioned behavior cloning (GCBC) baselines to demonstrate the value of UVD. Fixing a choice of visual representation, the only difference of GCBC to ours is the how the goals are labeled at training time. For each observation, GCBC labels the final frame in the same trajectory as its goal.

IL Evaluation Protocol. Our training and evaluation design for FrankaKitchen is structured as follows: we train on n combinations of object sequences with IND evaluation, reserving the remaining $24 - n$ task sequences for evaluation of unseen OOD scenarios. We use $n = 16$ by default unless otherwise mentioned. For a fair comparison, we utilize the same 3 random seen-unseen partitions, generated by 3 unique pre-defined seeds, for every set of runs.

To evaluate policy performance, we consider both the success rate on the overall task (**success**) as well as the number of subtasks accomplished (**completion**). The success criterion for each subtask is determined by the simulation ground-truth state; this is used solely during evaluations and is not provided to the agent during training. Results are presented in Table I.

Results. Remarkably, by using UVD, **_all_** pre-trained visual representation show significant improvement in OOD sequential generalization, despite their varying IND performances. VIP and LIV, the two representations explicitly trained to learn monotone embedding distances, demonstrate higher *comparative* gains compared to the other representations, despite similar or even lower performances when the representations are not used to decompose subgoals (i.e., GCBC-MLP); this validates our hypothesis that representations capturing visual task progress information are more suited for off-the-shelf subgoal discovery.
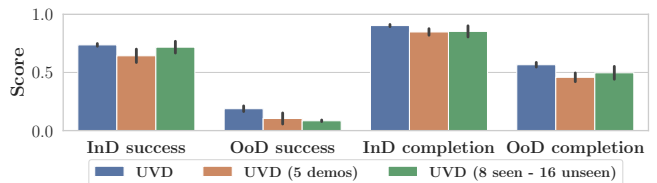

Fig. 4: **Ablations on dataset size and composition.**

Ablations. We present several ablations studying whether UVD remains effective when varying training settings. As VIP stands out as the most promising candidate for UVD-

Method	Success	Completion
GCRL-VIP	0.0 / 0.0	0.09 / 0.25
GCRL-VIP + Ours	**0.65 / 1.0**	**0.75 / 1.0**
GCRL-R3M	0.0 / 0.0	0.09 / 0.25
GCRL-R3M + Ours	**0.649 / 1.0**	**0.82 / 1.0**

TABLE II: **RL results on FrankaKitchen**. Full-stage success rate and the percentage of full-stage completion are reported in the format of (average performance with 3 random seeds) / (max performance).

Task	Method	IND S.	IND C.	OOD S.	OOD C.
Apple-in-Oven	GCBC	0.50	0.438	0.0	0.500
	GCBC + Ours	0.60	**0.750**	**0.25**	**0.625**
Fries-and-Rack	GCBC	0.30	0.567	0.0	0.0
	GCBC + Ours	0.35	**0.750**	**0.25**	**0.500**
Fold-Cloth	GCBC	0.05	0.100	0.0	0.0
	GCBC + Ours	0.15	**0.483**	**0.15**	**0.425**

TABLE III: **IND and OOD Results on Real-World Tasks.** S-success, C-completion.

based imitation learning, we perform all ablations using VIP as the backbone representation. First, we ablate the MLP policy architecture with a GPT-like causal transformer policy [45]. As shown in the last row of Table I, this more powerful, history-aware, policy is insufficient to achieve the same level of generalization; UVD again provides sizable generalization improvement.

Beyond policy architecture, we also study the effect of dataset size and diversity. To this end, we consider (1) reducing the training dataset size to 5 demonstrations per training task, and (2) reducing the number of training tasks to 8 but keeping the full number of demonstrations per task. Both IND and OOD performance remains similar, confirming that UVD enables OOD generalization that is robust to the varying sizes and diversity of the training data.
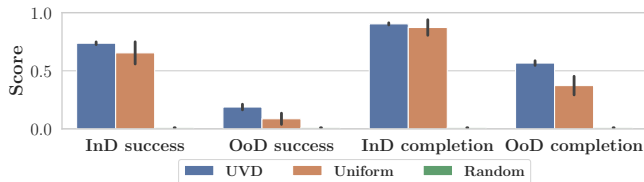

Fig. 5: **Comparison with heuristic goal-labeling methods.**

Finally, we study whether *UVD* is necessary to achieve strong OOD generalization and investigate alternative ways of generating subgoals. We consider **Uniform** and **Random**; **Uniform** randomly selects a frame within a fixed size window after the observation; this strategy has been employed in many prior works [16,30]. **Random** randomly selects 3 to 5 frames within the demonstration as subgoal frames. As shown in Fig. 5, the alternatives uniformly hurt performance on all settings and metrics. This is to be expected as these alternatives introduce redundant and less semantically meaningful subgoals; as a result, they may perform comparably IND, but their OOD generalization suffers.

UVD-Guided Reinforcement Learning. We investigate whether UVD can also enhance reinforcement learning by providing goal-based shaped rewards for subtasks (4). Recall that in this setting, only a single video demonstration (without action labels) is given to the agent to specify the learning task. Within the FrankaKitchen environment, we examine a specific task sequence: `open microwave`, `move kettle`, `toggle light switch`, and `slide cabinet`. We select VIP and R3M as candidate representations as they performed best for IL IND evaluations. We

consider a goal-conditioned RL baseline, which constructs goal-based rewards by uniformly using the last demonstration frame as goal in (4). We use PPO [46] as the RL algorithm and report the average and the max success rate and percentage of completion over 3 random seeds in Table II; see Appendix. 2. for more details.

We see baselines fail to make non-trivial task progress with either visual backbone, confirming that goal-based rewards with respect to a distant final goal are not well-shaped to guide exploration. In contrast, UVD-rewards consistently accelerate RL training and achieve high overall success on the task, validating UVD's utility in not only task generalization but also in task learning.

B. Real-World Experiments

We introduce 3 real-world multi-stage tasks on a real Franka robot. These tasks contain daily household manipulation skills, such as picking, pouring, folding, and manipulating articulated objects. See Fig. 7 for a detailed breakdown of the subtasks in each task. For each task, we have collected about 100 demonstrations via teleoperation; for each trajectory, the positions of relevant objects in the scene are randomized within a fixed distribution. The policies are learned via GCBC with MLP architecture as in simulation; see Appendix. E.4 for more real-robot details.

OOD Evaluation. On our real-world tasks, the subtasks are sequentially dependent and cannot be performed in arbitrary orders. To test compositional generalization, we evaluate whether the policies can *skip* intermediate tasks when their effects in the environment are already achieved. For example, on the `Fries-and-Rack` task, we evaluate on initial states in which the fries are already placed on the plate. In this case, a policy trained with semantically meaningful subgoals should be able to directly proceed from picking up the bowl to racking the bowl. This is because the post-condition of pouring the fries is semantically identical to the pre-condition of racking the bowl – both have the bowl picked up mid air and the fries on the plate. Similarly, on the `Apple-in-Oven` task, we test generalization by having the apple directly placed on the plastic plate, and on the `Fold-Cloth` task, we have the cloth folded diagonally already; see Figure 6 for an illustration of these OOD initial observations. While these OOD tasks are shorter than the training tasks, the exact sequences are still unseen during training and they contain unseen initial state configurations. As before, we test these OOD as well as IND task sequences;
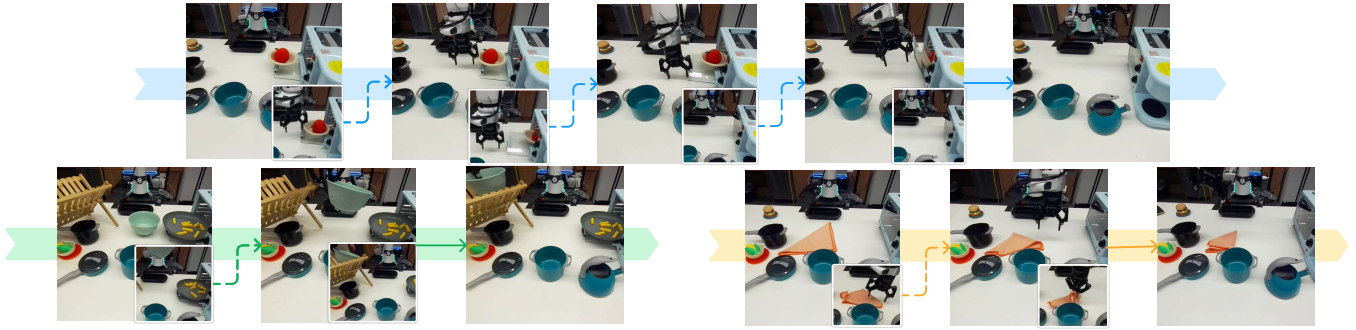
Fig. 6: **Example Sub-Sampled Rollouts on Real-World OOD Tasks.** The initial frame in each sequence is a representative OOD initial observation. The inset image in each frame is the conditioned UVD-discovered goal for that frame.
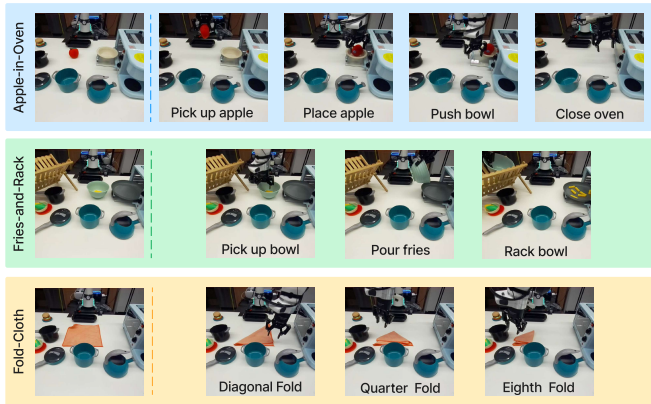

Fig. 7: **Real-World Tasks.** The first picture in each row depicts a representative initial observation, and the following frames are the distinct subtasks.

for each task sequence, we evaluate on 20 rollouts using the same set of object configurations for every compared method.

Results are presented in Table III. As shown, on all tasks, UVD methods can solve OOD tasks whereas the baseline completely fails, despite their comparable performance on IND tasks. These results corroborate our findings in simulation and make a strong case for the effectiveness of UVD's subgoals and its applicability to challenging real-world tasks. In addition to introducing OOD for initial states, we also show in Appendix 2. that our plug-and-play can recover from unexpected human interference in intermediate states. In contrast, GCBC struggles significantly in these situations. This underscores the ability of UVD's subgoals to guide the agent effectively in challenging OOD situations.

In Figure 6, we visualize UVD policy rollouts by displaying sub-sampled frames and their conditioned subgoals (the inset frame) on the OOD tasks. In all cases, UVD retrieves meaningful subgoals from the training set and the policy can successfully match the depicted semantic subtask.

VI. LIMITATION AND FUTURE WORKS

While UVD offers the advantage of not necessitating any task-specific knowledge or training, its efficacy is well-demonstrated across both simulated and real-robot environments. However, as we only validate on fully observable manipulation tasks, direct application to navigation tasks, especially those embodied tasks involving partial observations, may not yield intuitive or explainable subgoals (even though representations are pretrained with temporal objective using egocentric datasets [31,32,38]).

Looking ahead, we are eager to broaden the applications of UVD, diving deeper into its capabilities within egocentric scenarios, and even the key-frame extraction for video understanding and dense video caption tasks. On another front, while task graphs are widely used in Reset-Free RL [17,62], acquiring milestones as subgoals is resource-intensive and lacks scalability. By integrating our off-the-shelf UVD subgoals into the task-graph, we are interested in seeing agents that, with minimal resets, can adeptly handle a wide range of tasks across various sequences and horizons in the wild.

VII. CONCLUSION

We have presented Universal Visual Decomposer, an off-the-shelf task decomposition method for long-horizon visual manipulation tasks using pre-trained visual representations. UVD does not require any task-specific knowledge or training and effectively produces semantically meaning subgoals across both simulated and real-robot environments. UVD-discovered subgoals enable effective reward shaping for solving challenging multi-stage tasks using RL, and policies trained with IL exhibit significantly superior compositional generalization at test time.

REFERENCES

[1] P.-L. Bacon, J. Harb, and D. Precup, "The option-critic architecture," in *Proceedings of the AAAI conference on artificial intelligence*, vol. 31, no. 1, 2017. 2

[2] A. Bagaria and G. Konidaris, "Option discovery using deep skill chaining," in *International Conference on Learning Representations*, 2019. 2

[3] J. Borja-Diaz, O. Mees, G. Kalweit, L. Hermann, J. Boedecker, and W. Burgard, "Affordance learning from play for sample-efficient policy learning," in *2022 International Conference on Robotics and Automation (ICRA)*. IEEE, 2022, pp. 6372–6378. 1, 2

[4] E. Chane-Sane, C. Schmid, and I. Laptev, "Goal-conditioned reinforcement learning with imagined subgoals," in *International Conference on Machine Learning*. PMLR, 2021, pp. 1430–1440. 2

[5] L. Chen, K. Lu, A. Rajeswaran, K. Lee, A. Grover, M. Laskin, P. Abbeel, A. Srinivas, and I. Mordatch, "Decision transformer: Reinforcement learning via sequence modeling," *Advances in neural information processing systems*, vol. 34, pp. 15 084–15 097, 2021. 11

[6] J. Co-Reyes, Y. Liu, A. Gupta, B. Eysenbach, P. Abbeel, and S. Levine, "Self-consistent trajectory autoencoder: Hierarchical reinforcement learning with trajectory embeddings," in *International conference on machine learning*. PMLR, 2018, pp. 1009–1018. 2

[7] D. Damen, H. Doughty, G. M. Farinella, S. Fidler, A. Furnari, E. Kazakos, D. Moltisanti, J. Munro, T. Perrett, W. Price, *et al.*, "Scaling egocentric vision: The epic-kitchens dataset," in *Proceedings of the European conference on computer vision (ECCV)*, 2018, pp. 720–736. 1

[8] M. Deitke, W. Han, A. Herrasti, A. Kembhavi, E. Kolve, R. Mottaghi, J. Salvador, D. Schwenk, E. VanderBilt, M. Wallingford, L. Weihs, M. Yatskar, and A. Farhadi, "Robothor: An open simulation-to-real embodied AI platform," in *2020 IEEE/CVF Conference on Computer Vision and Pattern Recognition, CVPR 2020, Seattle, WA, USA, June 13-19, 2020*. Computer Vision Foundation / IEEE, 2020, pp. 3161–3171. [Online]. Available: https://openaccess.thecvf.com/content_CVPR_2020/html/Deitke_RoboTHOR_An_Open_Simulation-to-Real_Embodied_AI_Platform_CVPR_2020_paper.html 4

[9] J. Deng, W. Dong, R. Socher, L.-J. Li, K. Li, and L. Fei-Fei, "Imagenet: A large-scale hierarchical image database," in *2009 IEEE conference on computer vision and pattern recognition*. Ieee, 2009, pp. 248–255. 10, 11

[10] Y. Ding, C. Florensa, P. Abbeel, and M. Phielipp, "Goal-conditioned imitation learning," *Advances in neural information processing systems*, vol. 32, 2019. 3

[11] B. Eysenbach, R. R. Salakhutdinov, and S. Levine, "Search on the replay buffer: Bridging planning and reinforcement learning," *Advances in Neural Information Processing Systems*, vol. 32, 2019. 2

[12] K. Fang, P. Yin, A. Nair, and S. Levine, "Planning to practice: Efficient online fine-tuning by composing goals in latent space," in *2022 IEEE/RSJ International Conference on Intelligent Robots and Systems (IROS)*. IEEE, 2022, pp. 4076–4083. 1, 2

[13] K. Fang, P. Yin, A. Nair, H. R. Walke, G. Yan, and S. Levine, "Generalization with lossy affordances: Leveraging broad offline data for learning visuomotor tasks," in *Conference on Robot Learning*. PMLR, 2023, pp. 106–117. 1, 2

[14] D. Ghosh, A. Gupta, A. Reddy, J. Fu, C. Devin, B. Eysenbach, and S. Levine, "Learning to reach goals via iterated supervised learning," *arXiv preprint arXiv:1912.06088*, 2019. 3

[15] K. Grauman, A. Westbury, E. Byrne, Z. Chavis, A. Furnari, R. Girdhar, J. Hamburger, H. Jiang, M. Liu, X. Liu, *et al.*, "Ego4d: Around the world in 3,000 hours of egocentric video," in *Proceedings of the IEEE/CVF Conference on Computer Vision and Pattern Recognition*, 2022, pp. 18 995–19 012. 1

[16] A. Gupta, V. Kumar, C. Lynch, S. Levine, and K. Hausman, "Relay policy learning: Solving long-horizon tasks via imitation and reinforcement learning," *arXiv preprint arXiv:1910.11956*, 2019. 2, 4, 6

[17] A. Gupta, J. Yu, T. Z. Zhao, V. Kumar, A. Rovinsky, K. Xu, T. Devlin, and S. Levine, "Reset-free reinforcement learning via multi-task learning: Learning dexterous manipulation behaviors without human intervention," in *2021 IEEE International Conference on Robotics and Automation (ICRA)*. IEEE, 2021, pp. 6664–6671. 7, 15

[18] K. He, X. Zhang, S. Ren, and J. Sun, "Deep residual learning for image recognition," in *Proceedings of the IEEE conference on computer vision and pattern recognition*, 2016, pp. 770–778. 10

[19] M. Heo, Y. Lee, D. Lee, and J. J. Lim, "Furniturebench: Reproducible real-world benchmark for long-horizon complex manipulation," *arXiv preprint arXiv:2305.12821*, 2023. 2

[20] D.-A. Huang, S. Nair, D. Xu, Y. Zhu, A. Garg, L. Fei-Fei, S. Savarese, and J. C. Niebles, "Neural task graphs: Generalizing to unseen tasks from a single video demonstration," in *Proceedings of the IEEE/CVF conference on computer vision and pattern recognition*, 2019, pp. 8565–8574. 1, 2

[21] S. James and A. J. Davison, "Q-attention: Enabling efficient learning for vision-based robotic manipulation," *IEEE Robotics and Automation Letters*, vol. 7, no. 2, pp. 1612–1619, 2022. 1, 2

[22] D. Jayaraman, F. Ebert, A. A. Efros, and S. Levine, "Time-agnostic prediction: Predicting predictable video frames," *ICLR*, 2019. 2

[23] A. Karpathy, "nanogpt: The simplest, fastest repository for training/finetuning medium-sized gpts." 2023. [Online]. Available: https://github.com/karpathy/nanoGPT 11

[24] A. Khandelwal, L. Weihs, R. Mottaghi, and A. Kembhavi, "Simple but effective: Clip embeddings for embodied ai," in *Proceedings of the IEEE/CVF Conference on Computer Vision and Pattern Recognition*, 2022, pp. 14 829–14 838. 1

[25] P. Khosla, P. Teterwak, C. Wang, A. Sarna, Y. Tian, P. Isola, A. Maschinot, C. Liu, and D. Krishnan, "Supervised contrastive learning," *Advances in Neural Information Processing Systems*, vol. 33, pp. 18 661–18 673, 2020. 5

[26] Y. Lee, E. S. Hu, and J. J. Lim, "Ikea furniture assembly environment for long-horizon complex manipulation tasks," in *2021 ieee international conference on robotics and automation (icra)*. IEEE, 2021, pp. 6343–6349. 2

[27] Y. Lee, A. Szot, S.-H. Sun, and J. J. Lim, "Generalizable imitation learning from observation via inferring goal proximity," in *Advances in Neural Information Processing Systems*, A. Beygelzimer, Y. Dauphin, P. Liang, and J. W. Vaughan, Eds., 2021. [Online]. Available: https://openreview.net/forum?id=lp9foO8AFoD 12

[28] Y. Li, T. Gao, J. Yang, H. Xu, and Y. Wu, "Phasic self-imitative reduction for sparse-reward goal-conditioned reinforcement learning," in *International Conference on Machine Learning*. PMLR, 2022, pp. 12 765–12 781. 12

[29] I. Loshchilov and F. Hutter, "Decoupled weight decay regularization," *arXiv preprint arXiv:1711.05101*, 2017. 13, 15

[30] C. Lynch, M. Khansari, T. Xiao, V. Kumar, J. Tompson, S. Levine, and P. Sermanet, "Learning latent plans from play," in *Conference on robot learning*. PMLR, 2020, pp. 1113–1132. 6

[31] Y. J. Ma, W. Liang, V. Som, V. Kumar, A. Zhang, O. Bastani, and D. Jayaraman, "Liv: Language-image representations and rewards for robotic control," *arXiv preprint arXiv:2306.00958*, 2023. 1, 3, 5, 7, 15

[32] Y. J. Ma, S. Sodhani, D. Jayaraman, O. Bastani, V. Kumar, and A. Zhang, "Vip: Towards universal visual reward and representation via value-implicit pre-training," *arXiv preprint arXiv:2210.00030*, 2022. 1, 2, 3, 4, 5, 7, 10, 11, 12, 15

[33] A. Majumdar, K. Yadav, S. Arnaud, Y. J. Ma, C. Chen, S. Silwal, A. Jain, V.-P. Berges, P. Abbeel, J. Malik, *et al.*, "Where are we in the search for an artificial visual cortex for embodied intelligence?" *arXiv preprint arXiv:2303.18240*, 2023. 1

[34] A. Mandlekar, D. Xu, R. Martín-Martín, S. Savarese, and L. Fei-Fei, "Learning to generalize across long-horizon tasks from human demonstrations," *arXiv preprint arXiv:2003.06085*, 2020. 1, 2

[35] O. Nachum, S. Gu, H. Lee, and S. Levine, "Near-optimal representation learning for hierarchical reinforcement learning," *arXiv preprint arXiv:1810.01257*, 2018. 2

[36] O. Nachum, S. S. Gu, H. Lee, and S. Levine, "Data-efficient hierarchical reinforcement learning," *Advances in neural information processing systems*, vol. 31, 2018. 2

[37] S. Nair and C. Finn, "Hierarchical foresight: Self-supervised learning of long-horizon tasks via visual subgoal generation," *arXiv preprint arXiv:1909.05829*, 2019. 1, 2

[38] S. Nair, A. Rajeswaran, V. Kumar, C. Finn, and A. Gupta, "R3m: A universal visual representation for robot manipulation," *arXiv preprint arXiv:2203.12601*, 2022. 1, 3, 5, 7, 10, 11, 12, 15

[39] S. Nasiriany, V. Pong, S. Lin, and S. Levine, "Planning with goal-conditioned policies," *Advances in Neural Information Processing Systems*, vol. 32, 2019. 2

[40] A. Y. Ng, D. Harada, and S. Russell, "Policy invariance under reward transformations: Theory and application to reward shaping," in *Icml*, vol. 99, 1999, pp. 278–287. 12

[41] M. Oquab, T. Darcet, T. Moutakanni, H. Vo, M. Szafraniec, V. Khalidov, P. Fernandez, D. Haziza, F. Massa, A. El-Nouby, *et al.*, "Dinov2: Learning robust visual features without supervision," *arXiv preprint arXiv:2304.07193*, 2023. 5

[42] S. Parisi, A. Rajeswaran, S. Purushwalkam, and A. Gupta, "The unsurprising effectiveness of pre-trained vision models for control," *arXiv preprint arXiv:2203.03580*, 2022. 1

[43] K. Pertsch, O. Rybkin, F. Ebert, S. Zhou, D. Jayaraman, C. Finn, and S. Levine, "Long-horizon visual planning with goal-conditioned hierarchical predictors," *Advances in Neural Information Processing Systems*, vol. 33, pp. 17 321–17 333, 2020. 1, 2

[44] A. Radford, J. W. Kim, C. Hallacy, A. Ramesh, G. Goh, S. Agarwal, G. Sastry, A. Askell, P. Mishkin, J. Clark, *et al.*, "Learning transferable visual models from natural language supervision," in *International Conference on Machine Learning*. PMLR, 2021, pp. 8748–8763. 5, 10

[45] A. Radford, J. Wu, R. Child, D. Luan, D. Amodei, and I. Sutskever, "Language models are unsupervised multitask learners," 2019. 6

[46] J. Schulman, F. Wolski, P. Dhariwal, A. Radford, and O. Klimov, "Proximal policy optimization algorithms," *arXiv preprint arXiv:1707.06347*, 2017. 6, 12

[47] P. Sermanet, C. Lynch, Y. Chebotar, J. Hsu, E. Jang, S. Schaal, S. Levine, and G. Brain, "Time-contrastive networks: Self-supervised learning from video," in *2018 IEEE international conference on robotics and automation (ICRA)*. IEEE, 2018, pp. 1134–1141. 2

[48] N. M. Shafiullah, Z. Cui, A. A. Altanzaya, and L. Pinto, "Behavior transformers: Cloning k modes with one stone," *Advances in neural information processing systems*, vol. 35, pp. 22 955–22 968, 2022. 11

[49] L. X. Shi, A. Sharma, T. Z. Zhao, and C. Finn, "Waypoint-based imitation learning for robotic manipulation," *arXiv preprint arXiv:2307.14326*, 2023. 1, 2

[50] K. Shiarlis, M. Wulfmeier, S. Salter, S. Whiteson, and I. Posner, "Taco: Learning task decomposition via temporal alignment for control," in *International Conference on Machine Learning*. PMLR, 2018, pp. 4654–4663. 1, 2

[51] M. Shridhar, L. Manuelli, and D. Fox, "Perceiver-actor: A multi-task transformer for robotic manipulation," in *Conference on Robot Learning*. PMLR, 2023, pp. 785–799. 1, 2

[52] K. P. Singh, L. Weihs, A. Herrasti, J. Choi, A. Kembhavi, and R. Mottaghi, "Ask4help: Learning to leverage an expert for embodied tasks," *Advances in Neural Information Processing Systems*, vol. 35, pp. 16 221–16 232, 2022. 13

[53] J. Su, Y. Lu, S. Pan, A. Murtadha, B. Wen, and Y. Liu, "Roformer: Enhanced transformer with rotary position embedding," *arXiv preprint arXiv:2104.09864*, 2021. 11

[54] R. S. Sutton, D. Precup, and S. Singh, "Between mdps and semi-mdps: A framework for temporal abstraction in reinforcement learning," *Artificial intelligence*, vol. 112, no. 1-2, pp. 181–211, 1999. 2

[55] H. Takeda, S. Farsiu, and P. Milanfar, "Kernel regression for image processing and reconstruction," *IEEE Transactions on image processing*, vol. 16, no. 2, pp. 349–366, 2007. 10

[56] H. Touvron, L. Martin, K. Stone, P. Albert, A. Almahairi, Y. Babaei, N. Bashlykov, S. Batra, P. Bhargava, S. Bhosale, *et al.*, "Llama 2: Open foundation and fine-tuned chat models," *arXiv preprint arXiv:2307.09288*, 2023. 11

[57] L. Weihs, M. Deitke, A. Kembhavi, and R. Mottaghi, "Visual room rearrangement," in *IEEE Conference on Computer Vision and Pattern Recognition, CVPR 2021, virtual, June 19-25, 2021*. Computer Vision Foundation / IEEE, 2021, pp. 5922–5931. [Online]. Available: https://openaccess.thecvf.com/content/CVPR2021/html/Weihs_Visual_Room_Rearrangement_CVPR_2021_paper.html 4

[58] L. Weihs, J. Salvador, K. Kotar, U. Jain, K.-H. Zeng, R. Mottaghi, and A. Kembhavi, "Allenact: A framework for embodied ai research," *arXiv preprint arXiv:2008.12760*, 2020. 12

[59] E. Wijmans, A. Kadian, A. Morcos, S. Lee, I. Essa, D. Parikh, M. Savva, and D. Batra, "DD-PPO: learning near-perfect pointgoal navigators from 2.5 billion frames," in *8th International Conference on Learning Representations, ICLR 2020, Addis Ababa, Ethiopia, April 26-30, 2020*. OpenReview.net, 2020. [Online]. Available: https://openreview.net/forum?id=H1gX8C4YPr 4

[60] T. Xiao, I. Radosavovic, T. Darrell, and J. Malik, "Masked visual pre-training for motor control," *arXiv preprint arXiv:2203.06173*, 2022. 1

[61] D. Xu, S. Nair, Y. Zhu, J. Gao, A. Garg, L. Fei-Fei, and S. Savarese, "Neural task programming: Learning to generalize across hierarchical tasks," in *2018 IEEE International Conference on Robotics and Automation (ICRA)*. IEEE, 2018, pp. 3795–3802. 1, 2

[62] K. Xu, Z. Hu, R. Doshi, A. Rovinsky, V. Kumar, A. Gupta, and S. Levine, "Dexterous manipulation from images: Autonomous real-world rl via substep guidance," in *2023 IEEE International Conference on Robotics and Automation (ICRA)*. IEEE, 2023, pp. 5938–5945. 7, 15

[63] B. Zhang and R. Sennrich, "Root Mean Square Layer Normalization," in *Advances in Neural Information Processing Systems 32*, Vancouver, Canada, 2019. [Online]. Available: https://openreview.net/references/pdf?id=S1qBAf6rr 11, 13

[64] L. Zhang, G. Yang, and B. C. Stadie, "World model as a graph: Learning latent landmarks for planning," in *International Conference on Machine Learning*. PMLR, 2021, pp. 12 611–12 620. 2

[65] Z. Zhang and L. Weihs, "When learning is out of reach, reset: Generalization in autonomous visuomotor reinforcement learning," *arXiv preprint arXiv:2303.17600*, 2023. 12, 13

A DETAILS ON UVD

1. Decomposition

As we show in Algo. 1, UVD preprocesses the demonstration or user-provided raw video offline. We further provide low-level pseudocode in Python of UVD in Pseudocode. A.1. In practice, when identifying the temporally nearest observation where the monotonicity condition is not met, as per Eq. 3, it is equivalent to locating the most recent local maximum of the embedding distance curves. This is because the distance curve is anticipated to show an almost monotonically decreasing trend towards the final frame in each recursive iteration, as shown in Eq. 2. Due to the small-scale noise in pixel and high-dimensional feature space, we apply Nadaraya-Watson Kernel Regression [55] to first smooth the embedding curves before calculating the embedding distances. We benchmark our UVD implementation runtime in Appendix. A4., which shows a negligible time span, even when handling high-resolution videos with substantial duration in the wild.

```python
from scipy.signal import argrelextrema

def UVD(
    embeddings: np.ndarray | torch.Tensor,
    smooth_fn: Callable,
    min_interval: int,
) -> list[int]:
    # last frame as the last subgoal
    cur_goal_idx = -1
    # saving (reversed) subgoal indices (timesteps)
    goal_indices = [cur_goal_idx]
    cur_emb = embeddings.copy() # L, d
    while cur_goal_idx > min_interval:
        # smoothed embedding distance curve (L,)
        d = norm(cur_emb - cur_emb[-1], axis=-1)
        d = smooth_fn(d)
        # monotonicity breaks (e.g. maxima)
        extremas = argrelextrema(d, np.greater)[0]
        extremas = [
            e for e in extremas
            if cur_goal_idx - e > min_interval
        ]
        if extremas:
            # update subgoal by Eq.(3)
            cur_goal_idx = extremas[-1] - 1
            goal_indices.append(cur_goal_idx)
            cur_emb = embeddings[:cur_goal_idx + 1]
        else:
            break
    return embeddings[
        goal_indices[::-1]  # chronological
    ]
```

Pseudocode A.1: **UVD implementation in Python**

In all of our simulation and real-world experiments, we use `min_interval` $= 20$, and Radial Basis Function (RBF) with the bandwidth of 0.08 for Kernel Regression, to eliminate most of the visual and motion noise in the video. We provide UVD decomposition qualitative results in Appendix. F.

2. Inference

We now elucidate the specifics of applying UVD subgoals in a multi-task setting during inference. Remember that given a video demonstration represented as $\tau = (o_0, \cdots, o_T)$ and UVD-identified subgoals $\tau_{goal} = (g_0, \cdots, g_m)$, we can extract an augmented trajectory labeled with goals, represented as $\tau_{aug} = (o_a, a_0, g_0), \cdots, o_T, a_T, g_m$. This is useful for goal-conditioned policy training, as discussed in Sec. IV-B.

For inference, we can similarly produce an augmented offline trajectory without the necessity of ground-truth actions, i.e., $\tau_{aug,infer} = \{(o_0, g_0), \cdots, (o_T, g_m)\}$. In the online rollout, after resetting the environment to o_0, the agent continuously predicts and enacts actions conditioned on subgoal g_0 using the trained policy. This continues until the embedding distance between the current observation and the subgoal surpasses a pre-set positive threshold ϵ at a specific timestep i, *i.e.* $d_\phi(o_i; g_0) < \epsilon$, where ϕ is the same frozen visual backbone used in decomposition and training. Following this, the subgoal will be seamlessly transitioned to the next, continuing until success or failure is achieved.

In practice, the straightforward goal-relaying inference method might face accumulative errors during multiple subgoal transitions, especially due to noise from online rollouts. However, when an agent is guided explicitly by tasks depicted in a video, incorporating the duration dedicated to each subgoal can help reduce this vulnerability. To clarify, once we've aligned subgoals with observations from the video, we also draw a connection between the timesteps of observations and their corresponding subgoals. We denote the *subgoal budget* for subgoal $g_i = o_t$ as $\mathcal{B}_{g_i} := n + 1$ where $g_{i-1} = o_{t-n-1}$ based on Eq. 3. Building on this, we propose a secondary criterion for switching subgoals: verify if the relative steps completing the current stage are in the neighborhood of the subgoal budget. This measure ensures timely transitions: it avoids prematurely switching before completing a sub-stage or delaying the transition despite accomplishing the sub-stage in the environment. To sum up, given an ongoing observation o_t and subgoal g_i at timestep t, and considering the preceding subgoal g_{i-1} at timesteps $t - h$, the subgoal will transition to g_{i+1} if

$$d_\phi(o_t; g_i) < \epsilon \quad \text{and} \quad |h - \mathcal{B}_{g_i}| < \delta \qquad (5)$$

We use $\epsilon = 0.2$ and $\delta = 2$ steps for all of our experiments, except in baseline tests that are conditioned solely on final goals.

3. Feature Continuity

We then visualize 3D t-SNE in feature space from different frozen visual backbones in Fig. A.1. We include VIP [32], R3M [38], CLIP [44], and ResNet [18] trained for ImageNet-1k classification [9]. As shown in Fig. A.1, representations pretrained with temporal objectives, *e.g.* VIP [32] and R3M [38], provide more smooth, continuous, and monotone clusters than other vision foundation models. In practice, those representations with more smooth and continuous embedding curves provide better UVD decomposition as well as better performance in downstream control.

4. Runtime of UVD

Finally, We present the average runtime of UVD for preprocessing and decomposing trajectories. We break the
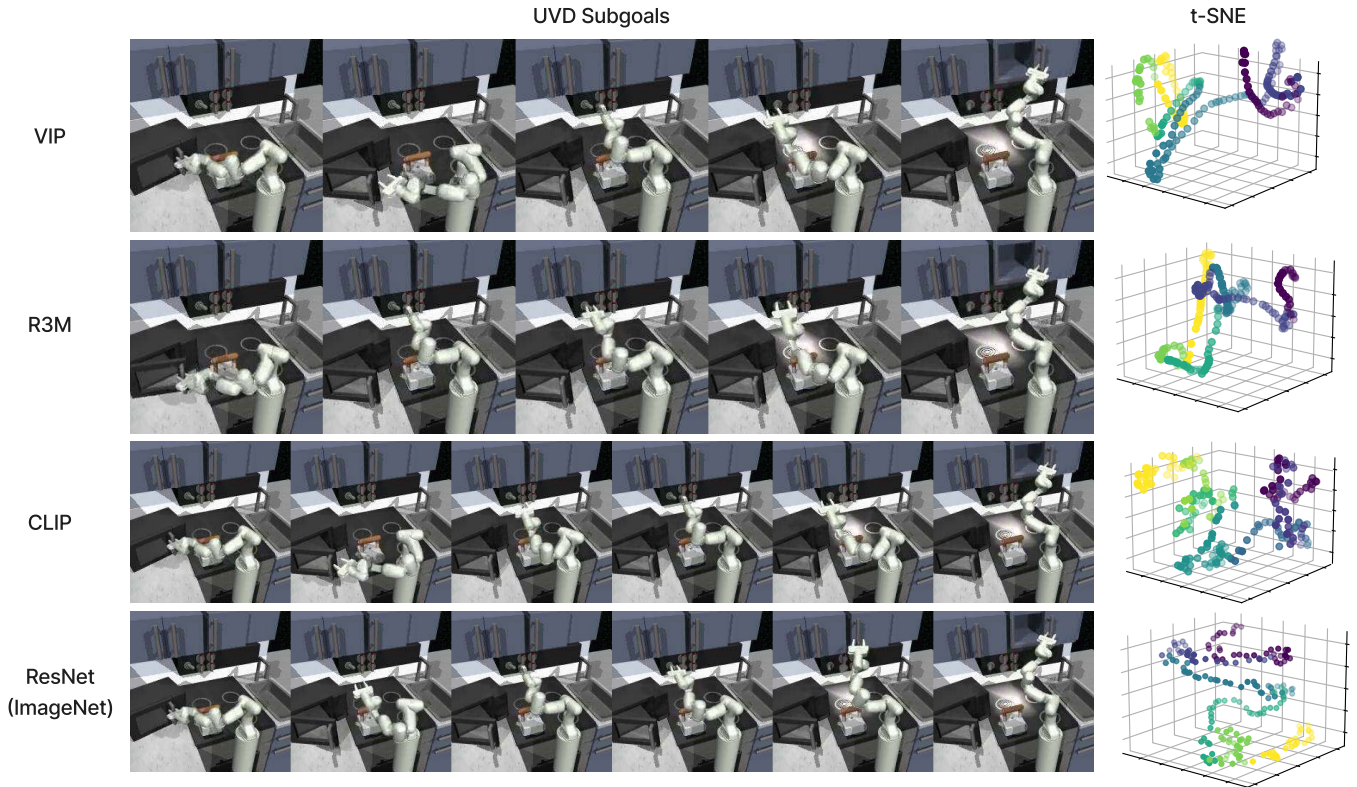
Fig. A.1: **UVD subgoals and 3D t-SNE visualizations of different frozen visual embeddings.** t-SNE colors are labeled by UVD subgoals. Representations pretrained with temporal objectives like VIP [32] and R3M [38] provide more smooth, continuous, and monotone clusters in feature space than others, whereas the ResNet trained for supervised classification on ImageNet-1k [9] provide the most sparse embeddings.

runtime by: 1) **load** from raw video file into an array; 2) **preprocess** the video array by the frozen visual encoder (including the tensor and device conversions); and 3) apply **UVD** to the preprocessed embeddings. In addition to the FrankaKitchen dataset and real-world data used for our experiments, we assessed the decomposition capabilities on a 720P MOV video. The video has a frame rate of 30 fps, contains 698 frames (equating to a duration of 23.3 seconds), and is decomposed into 16 subgoals. Visualizations can be found in Fig. F.15. Runtimes were calculated based on an average of 513 episodic data from the FrankaKitchen dataset and 100 trials for the `in the wild` video, all processed on an RTX A6000 GPU. Preprocessing is required only once offline before the policy training. As indicated in Tab. A.1, UVD operates in a negligible time span, even when handling high-resolution videos with substantial duration in the wild.

	# frames	Load	Preprocess	UVD
FrankaKitchen	226.9	0.023	0.155	0.0023
In the wild	698	1.011	0.450	0.011

TABLE A.1: **UVD offline preprocess runtimes (in seconds).**

B MODELS

1. Policies

To underscore that our method serves as an off-the-shelf method that is applicable to different policies, we ablate with a Multilayer Perceptron (MLP) based single-step policy and a GPT-like causal transformer policy. We summarize the MLP and GPT policies hyperparameters in Tab. C.4 C.5. The MLP policy, akin to the designs in [32,38] for downstream control tasks, employs a 3-layer MLP with hidden sizes of [1024, 512, 256] to produce deterministic actions. This MLP ingests a combination of the frozen visual embeddings from stepwise RGB observations and goal images followed by a 1D BatchNorm, as well as the 9D proprioceptive data encoded through a single layer complemented by a LayerNorm.

Our GPT policy removes the BatchNorm and replaces the MLP with the causal self-attention blocks consisting of 8 layers, 8 heads, and an embedding dimension of 768. We set an attention dropout rate of 0.1 and a context length of 10. The implementation is built upon [23,56]. We transition from the conventional LayerNorm to the Root Mean Square Layer Normalization (RMSNorm) [63] and enhance the transformer with rotary position embedding (RoPE) [53]. Actions are predicted via a linear similar to [5]. In practice, we generally found this recipe has more stable training and better performance than the original implementation from [23,48]. At inference time, we cache the keys and

values of the self-attention at every step, ensuring that there's no bottleneck as the context length scales up. Nevertheless, in the FrankaKitchen tasks, we observed that a longer context length tends to overfit and performance drop. Therefore, we consistently use a context length of 10 for all experiments.

Policy	MLP	MLP + UVD	GPT	GPT + UVD
Episodic Runtime	6.03	6.17	7.43	7.50

TABLE B.2: **Benchmark the inference runtime (in seconds).** Runtimes are averaged across 100 rollouts with one GPU process and episodic horizon 300.

C TRAINING DETAILS

1. Imitation Learning

We summarize the hyperparameters of imitation learning in Tab. C.3. In the simulation, we conduct an online evaluation every 100 epochs using 10 parallel environments for each GPU machine. We choose the best checkpoints based on the combined IND and OOD performance, averaged across all multi-task training scenarios. For benchmarking inference time, we employ a single GPU, comparing our approach with the GCBC baseline as shown in Tab. B.2. This further underscores that UVD incurs negligible overhead throughout the preprocessing, training, and inference stages.

2. Reinforcement Learning

All RL experiments are trained using the Proximal Policy Optimization (PPO) [46] RL algorithm implemented within the AllenAct [58] RL training framework. We summarize the hyperparameters of reinforcement learning in Tab. C.6.

In our RL setting, the configurations for both training and inference remain consistent. This is analogous to the inference for IL as detailed in Appendix. A2.. Specifically, the task is also specified by an unlabeled video trajectory τ. Given the initial observation o_0 and UVD subgoal $g_0 \in \tau_{goal}$, the agent continuously predicts and executes actions conditioned on subgoal g_0 using the online policy with frozen visual encoder ϕ, until the condition $d_\phi(o_t; g_0) < \epsilon$ satisfied for some timestep t and positive threshold ϵ.

As shown in Eq. 4, we provide progressive rewards defined as goal-embedding distance *difference* using UVD subgoals. Recognizing that the distance between consecutive subgoals can vary, we employ the normalized distance function: $\bar{d}_\phi(o_t; g_i) := d_\phi(o_t; g_i)/d_\phi(g_{i-1}; g_i)$. This ensures that $\bar{d}_\phi(o_{t-h}; g_i) \approx 1$ for some timestep $t - h$ that the subgoal was transitioned from g_{i-1} to g_i. Additionally, we provide modest discrete rewards for encouraging (chronically) subgoal transitions, and larger terminal rewards for the full completion of task sub-stages, which is equivalent as the embedding distance between the observation and the final subgoal becomes sufficiently small. To sum up, at timestep t, the agent is receiving a weighted reward

$$
\begin{aligned}
R_t = \alpha \cdot \big(\bar{d}_\phi(o_{t-1}; g_i) - d_\phi(o_t; g_i) \big) \\
+ \beta \cdot \mathbf{1}_{\bar{d}_\phi(o_t; g_i) < \epsilon} \\
+ \gamma \cdot \mathbf{1}_{\bar{d}_\phi(o_t; g_m) < \epsilon}
\end{aligned} \tag{6}
$$

based on the RGB observations o_t, o_{t-1}, corresponding UVD subgoal $g_i \in \tau_{goal}$, and final subgoal $g_m \in \tau_{goal}$. While similar reward formulations appear in works such as [27,28,32,40,65], we are the first in delivering optimally monotonic implicit rewards unsupervisedly by UVD, derived directly from RGB features. In our experiments, we use $\alpha = 5, \beta = 3, \gamma = 6, \epsilon = 0.2$, and confine the first term within the range $[-\alpha, \alpha]$ in case edge cases in feature space. For the final-goal-conditioned RL baseline, it is equivalent as $g_i = g_m = o_T \in \tau = \{o_0, \cdots, o_T\}$ and $\beta = 0$ in Eq. 6.

Tab. II illustrates that the simple incorporation of UVD-rewards greatly enhances performance. We also showcase a comparison of evaluation rewards between GCRL and GCRL augmented with our UVD rewards. This is done using the R3M [38] and VIP [32] backbones, as seen in Fig. C.2. This highlights the capability of our UVD to offer more streamlined progressive rewards. This capability is pivotal for the agent to adeptly manage the challenging, multi-stage tasks presented in FrankaKitchen. To the best of our knowledge, ours is the first work to achieve such a high success rate in the FrankaKitchen task without human reward engineering and additional training. Notably, our RL agent, trained with the optimally monotonic UVD-reward, can complete 4 sequential tasks in as few as **90 steps** — a stark contrast to the over 200 steps observed in human-teleoperated demonstrations. This further illustrates the UVD-reward's potential to encourage agents to accomplish multi-stage goals more efficiently. The videos of rollouts can be found on our website.
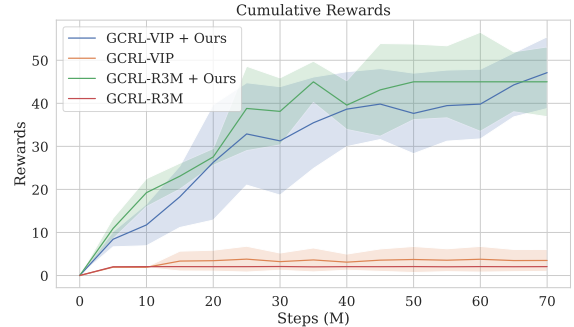

Fig. C.2: **RL evaluation cumulative rewards.** Note that different visual backbones may not be comparable due to different representation spaces, but we show significant progressive signals in comparison with the final-goal-conditioned baseline.

Failures in the GCRL baselines predominantly stem from the agent's tendency to get trapped in local minima, usually when it achieves a task sub-stage that results in the most significant visual changes in the feature space, *e.g.* sliding the cabinet in this case. Since it causes the most noticeable shifts both in pixel and feature representations, the baseline agent often fixates on this subtask alone, making no further progress. Conversely, when employing UVD subgoals and rewards, we have observed a marked difference during training. The agent incrementally learns to navigate the entire task, approaching it stage by stage. These stages are not

Hyperparameter/Value	MLP-Policy	GPT-Policy
Optimizer	AdamW [29]	AdamW [29]
Learning Rate	3e-4	3e-4
Learning Rate Schedule	cos decay	cos decay
Warmup Steps	0	1000
Decay Steps	150k	200k
Weight Decay	0.01	0.1
Betas	[0.9, 0.999]	[0.9, 0.99]
Max Gradient Norm	1.0	1.0
Batch Size	512	128

TABLE C.3: **IL training hyperparameters**

Hyperparameter	Value
Hidden Dim.	[1024, 512, 256]
Activation	ReLU
Proprio. Hidden dim.	512
Proprio. Activation	Tanh
Visual Norm.	Batchnorm1d
Proprio. Norm.	LayerNorm
Action Activation	Tanh
Trainable Parameters	3.3M

TABLE C.4: **MLP policy hyperparameters**

Hyperparameter	Value
Context Length	10
Embedding Dim.	768
Layers	8
Heads	8
Embedding Dropout	0.0
Attention Dropout	0.1
Normalization	RMSNorm [63]
Action Activation	Tanh
Trainable Parameters	58.6M

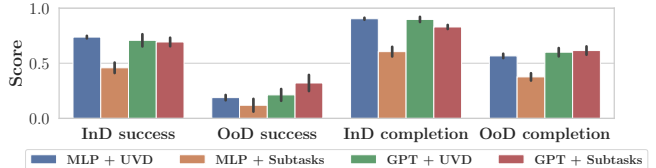TABLE C.5: **GPT policy hyperparameters**

Hyperparameter	Value
GPU instances	8x RTX A6000
Environments per GPU	8
Optimizer	AdamW [29]
Learning rate	3e-4
Learning rate schedule	linear decay
Max gradient norm	0.5
Discount factor γ	0.99
GAE τ	0.95
Value loss coefficient	0.5
Normalized advantages	True
Entropy coefficient	0.001
Rollout length	200
PPO epochs	10
Number of mini-batches	1
PPO Clip	0.1

TABLE C.6: **RL hyperparameters.**

Fig. D.3: **Comparison with the decomposition from human pre-defined**

isolated, as they share pertinent information. For example, UVD breaks down task sequences into phases characterized by nearly monotonic motions. These can be categorized as the "hand reaching" or "object interaction" phases. This shared knowledge framework means that once the agent masters the initial "hand reaching" phase, subsequent similar hand-reaching motions become more intuitive to learn and execute. Nevertheless, we do occasionally observe instances where applying UVD results in failure. In these cases, the agent often oscillates its gripper back and forth, seemingly hacking the reward shaping, which in turn leads to an irreversible state. We speculate that incorporating supervised human intervention [52] or unsupervised near-irreversible detection [65], could address this issue and further enhance performance.

D EXTENDED EXPERIMENTS AND ABLATIONS

1. Simulation

We present numerical results for ablations from Sec. V-A in Tab. D.7, with extended comparison with GCBC baselines. Without surprise, our method consistently outperforms baselines in compositional generalization settings, when varying the dataset size to 5 demonstrations for each FrankaKitchen task, or adjusting the seen-unseen partitions, which doubles the count of unseen sequences while halving the number of seen ones.

In the FrankaKitchen demonstrations, there are 24 task sequences encompassing 4 subtasks each, translating to 4 or-

dered object interactions. We further compare GCBC+UVD with GCBC conditioned on the final frames of each human-defined subtask in FrankaKitchen, utilizing both MLP and GPT policies. The main distinction between UVD-decomposed subgoals and the subgoals for each subtask is that UVD furnishes milestones emphasizing monotone motions, while subtasks yield subgoals with oracle semantic meanings. Both methodologies employ the identical inference approach as described in Appendix 2., and share the same tasks partitions from three distinct seeds. The average successes and subtask completion rates are shown in Fig. D.3. Surprisingly, even when subgoals from subtasks offer ground-truth semantic meaning (and, notably, share identical conditioned subgoal frames across different task sequences), only GPT policy allows for performance surpassing our method in the OoD setting. In the InD setting, however, using subgoals from pre-defined sub-tasks leads to a substantial performance drop for MLP policies. This decline might be due to potential confusion (*e.g.* mis-manipulated top and bottom burners) arising from similar subgoals when jointly training multiple multi-stage tasks when utilizing a lightweight, single-step MLP policy.

2. Real-Robot

In the OoD settings, even though we have not achieved exceptionally high success rates for all of the tasks, we still managed a completion rate of around or above 50%. This outcome can be attributed to the fact that policies trained using our method consistently exhibit the right intent. Instead of overfitting to the InD settings, they tend to successfully complete intermediate steps and occasionally face challenges only at later stages. In contrast, the GCBC baseline always overfits the InD initial state. For example, in Fold-Cloth generalization experiments, the baseline still goes to the corner that is already folded. For more rollout visualizations,

Representation	Method	IND success	IND completion	OOD success	OOD completion
VIP (5 demos)	GCBC-GPT	0.409 (0.102)	0.702 (0.066)	0.005 (0.005)	0.285 (0.024)
	GCBC-GPT + Ours	**0.419 (0.027)**	**0.763 (0.016)**	**0.13 (0.033)**	**0.533 (0.026)**
VIP (5 demos)	GCBC-MLP	**0.668 (0.024)**	0.82 (0.035)	0.016 (0.016)	0.208 (0.006)
	GCBC-MLP + Ours	0.643 (0.058)	**0.848 (0.028)**	**0.104 (0.048)**	**0.458 (0.038)**
VIP (8 seen - 16 unseen)	GCBC-MLP	0.724 (0.057)	0.851 (0.036)	0.001 (0.001)	0.102 (0.020)
	GCBC-MLP + Ours	0.717 (0.051)	0.853 (0.048)	**0.084 (0.007)**	**0.497 (0.055)**
VIP (8 seen - 16 unseen)	GCBC-GPT	0.602 (0.114)	0.554 (0.48)	0.003 (0.003)	0.143 (0.124)
	GCBC-GPT + Ours	0.587 (0.049)	0.558 (0.483)	**0.037 (0.040)**	**0.307 (0.268)**

TABLE D.7: **Ablations on dataset size and compositions, with comparisons with GCBC baselines and UVD**

please refer to the videos available on our website.

We further extend our OoD setting, which aimed for unseen initial states in Sec. V-B, also encompass more diverse intermediate states. Our objective during deployment is to ensure the agent remains resilient to tasks, even in the presence of human interference. In Apple-in-Oven and Fries-and-Rack tasks, we introduce two more OoD scenarios. In the first, we revert the scene by placing the apple back to its original position, challenging the agent to recover from this change. In the second, we manually circumvent an intermediate step. For instance, after the robot has grasped the bowl of fries, we manually transfer all the fries to the plate. This alteration means the agent should subsequently place the bowl directly on the rack without the need for pouring.

Method	Apple-in-Oven	Fries-and-Rack
GCBC	0.0	0.2
GCBC + Ours	**0.5**	**0.9**

TABLE D.8: **Success rate over 10 rollouts with human interference.**

E REAL-WORLD ROBOT EXPERIMENT DETAILS

The robot learning environment is illustrated in Fig. E.4. We use a 7-DoF Franka robot with a continuous joint-control action space. A Zed 2 camera is positioned on the table's right edge, and only its RGB image stream—excluding depth information—is employed for data collection and policy learning. Another Zed mini camera is affixed to the robot's wrist. For the Apple-in-Oven task, we utilize the right view from both cameras, while for the Fries-and-Rack and Fold-Cloth tasks, we rely on their left views.

1. Task Descriptions

	EL	# demos
Apple-in-Oven	197.5	105
Fries-and-Rack	170.1	110
Fold-Cloth	246.8	105

TABLE E.9: **Real Tasks average episode length (EL) and the number of demos (# demos).**

We specify the average episode lengths and the number of demonstrations we used for experiments for each task in

Fig. E.4: **Real robot experiments setup.**

Tab. E.9. The criteria for successful task completion are as follows:

- Apple-in-Oven: pick up the apple on the table; place the apple in the bowl without tipping it over; push the bowl into the oven; close the oven door.
- Fries-and-Rack: pour fries onto the plate, ensure at least half of them are on the plate; place the bowl on the rack without causing any collisions.
- Fold-Cloth: grasp the corner of the cloth and fold the cloth in the directions shown in the demonstrated video multiple times.

During evaluation, we assess the successful completion of each sub-stage over 20 rollouts to determine the overall success and completion rates. To evaluate our policy's compositional generalization abilities, we introduce unseen initial states for each task. While the success criteria remain consistent with prior assessments, the initial step has been pre-completed by humans. The extended OoD setting, which includes human interference in intermediate states, is detailed in Appendix 2..

2. Training and evaluation details

UVD in training: As with our simulation experiments, we preprocess all the demos using UVD. The behavior cloning policy further incorporates the view from the wrist camera besides the view from the side camera and decomposed

Fig. E.5: **Raw observations from two different cameras for three tasks.** Three (No.1, 3, 5 from the left) are from the side-view Zed2 camera and the others (No.2, 4, 6) are from Zed mini on the wrist.

subgoals during training. Operating under velocity control, our robot's action space encompasses a 6-DoF joint velocity and a singular dimension of the gripper action (open or close). Consequently, the policy produces 7D continuous actions. The robot control frequency is set as 15 Hz.

UVD in evaluating: In the training stage, we save the set of subgoals and corresponding observations over all demos in a task. During inference, every time the robot gets a pair of observations, we retrieve the subgoal that has the nearest observation (l_2 norm over observation embeddings) with the current one as the current subgoal. Then we concatenate the current observation with the retrieved subgoal together as input then get real-time joint velocity action.

Our method frequently results in the development of more robust policies, enabling recovery actions when initial attempts fail. For example, in the failure scenario of `Apple-in-Oven` and one of the successful cases in `Fold-Cloth` as showcased on our website, the policy opts for a reattempt, pushing the bowl further if not adequately placed inside the oven, or re-folding if the cloth's corner is not grasped properly. In contrast, such recovery behaviors are conspicuously absent in the GCBC baselines, further highlighting its propensity to overfit to IND training setting.

BC Model details: We train our policy on a laptop with RTX 3080 GPU. For both the baseline policy and our method, we add proprioception to help learning and augment each training dataset by randomly cropping the input images. Since we have limited demonstrations in the real world, we only set MLP size to be [256,256]. Please refer to Tab. E.10 for details.

Hyperparameter	Value
GPU Instances	RTX 3080 Ti Laptop GPU
MLP Architecture	[256, 256]
Non-Linear Activation	ReLU
Optimizer	AdamW [29]
Gradient Steps	10k
Batch Size	64
Learning Rate	1e-3
Proprioception	Yes
Augmentation	Random crop

TABLE E.10: **Real robot BC hyperparameters.**

F QUALITATIVE SUBGOAL DECOMPOSITION RESULTS

We show decomposition results with UVD on simulation videos in Fig. F.6 F.7, real robots videos in Fig. F.8, F.9, F.10, and wild videos in Fig. F.11, F.12, F.13, F.14, F.15. From

the subgoal decomposition results, we can have a clear overview of the key frames within a video. For instance, in `Fold-Cloth` video, UVD precisely catches the picking and placing key frames for three times.

Fig. F.6 F.7 are from our simluation experiments, Fig. F.8, F.9, F.10 are from real robot experiments. Fig. F.11 video depicts a human opening a cabinet and rearranging items, while Fig. F.12 video showcases unlocking a computer in an office. Furthermore, Fig. F.13 demonstrates the process of opening a drawer and charging a device, and Fig. F.14 illustrates washing and then wiping hands in a bathroom. Lastly, Fig. F.15 presents activities shot in the kitchen with relatively longer duration. Based on the analysis of all video decomposition results, it is evident that UVD extends beyond robotic settings, proving to be highly effective in household scenarios captured in human videos.

G LIMITATION AND FUTURE WORKS

While UVD offers the advantage of not necessitating any task-specific knowledge or training, its efficacy is well-demonstrated across both simulated and real-robot environments. However, as we only validate on fully observable manipulation tasks, direct application to navigation tasks, especially those embodied tasks involving partial observations, may not yield intuitive or explainable subgoals (even though representations are pretrained with temporal objective using egocentric datasets [31,32,38]).

Looking ahead, we are eager to broaden the applications of UVD, diving deeper into its capabilities within egocentric scenarios, and even the key-frame extraction for video understanding and dense video caption tasks. On another front, while task graphs are widely used in Reset-Free RL [17,62], acquiring milestones as subgoals is resource-intensive and lacks scalability. By integrating our off-the-shelf UVD subgoals into the task-graph, we are interested in seeing agents that, with minimal resets, can adeptly handle a wide range of tasks across various sequences and horizons in the wild.

Fig. F.6: **Video sequence**: moving a kettle, turning on light switch, operating slide cabinet, operating hinge cabinet.
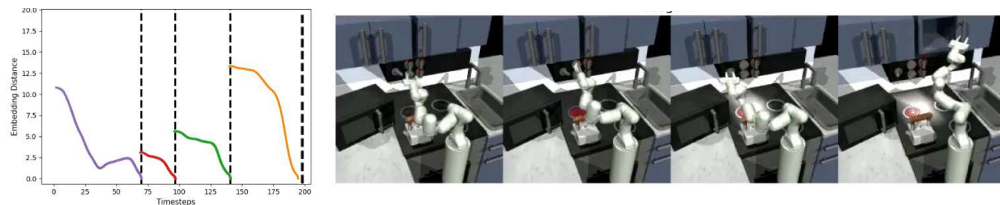

Fig. F.7: **Video sequence**: rotating bottom burner, rotating top burner, turning on light switch, operating slide cabinet.

Fig. F.8: **Video sequence**: picking apple, placing apple in the bowl, pushing the bowl into the oven, closing the oven.

Fig. F.9: **Video sequence**: picking a bowl, pour fries out of the bowl, placing the bowl on the rack.

Fig. F.10: **Video sequence**: diagonal fold, quarter fold, eighth fold.

Fig. F.11: **Video sequence**: picking upper white box, placing white box, picking upper black box, closing the cabinet.

Fig. F.12: **Video sequence**: grabbing a chair, moving the keyboard towards human, typing password, unlocking a computer.
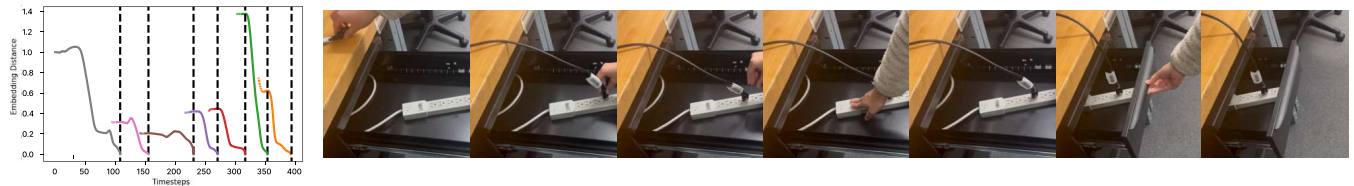

Fig. F.13: **Video sequence**: opening a drawer, picking the charger, plugging the charger, turning on the power strip, closing the drawer partially.

Fig. F.14: **Video sequence**: lathering hands, washing hands, turning off the tap, wiping hands with towel, placing back the cloth.
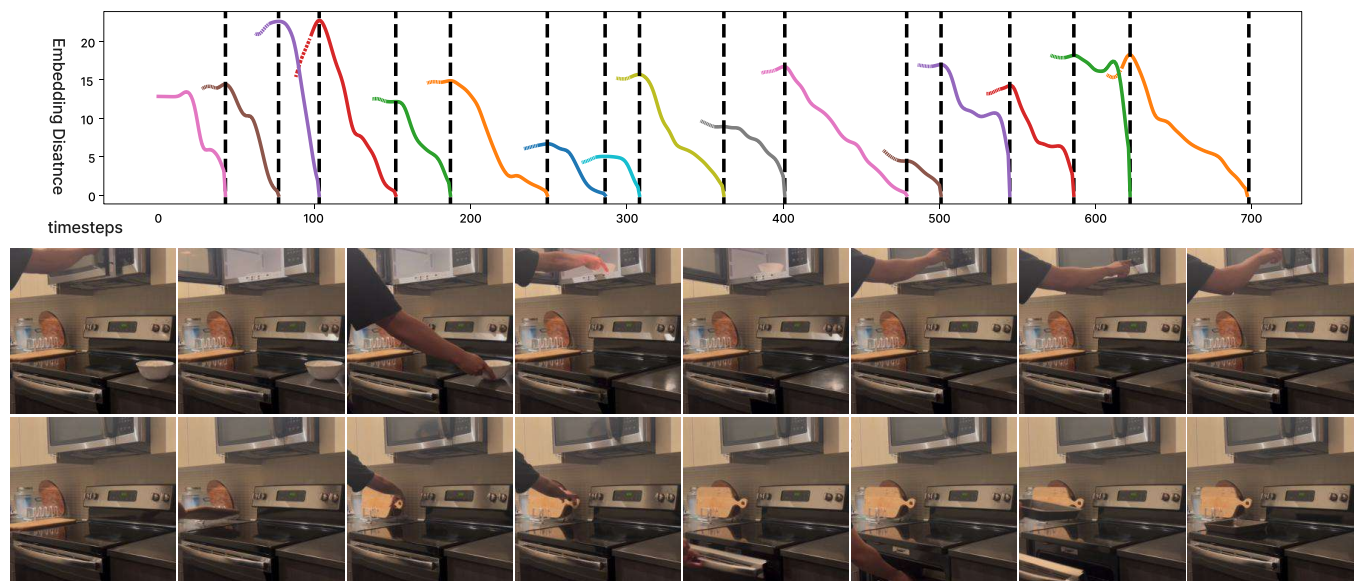

Fig. F.15: **UVD decomposes long video into subgoals.** The video sequence demonstrates: opening the microwave, placing a bowl with rice inside the microwave, closing the microwave, activating the microwave to heat the rice, placing the cutting board onto its rack, opening the oven, and putting the baking tray on the burner.